Fast calculation method for optical diffraction on tilted planes by use of the angular spectrum of plane waves

Fast calculation method for optical diffraction on tilted planes by use of the angular spectrum of plane waves

Kyoji Matsushima

Department of Electrical Engineering, Kansai University, 3-3-35 Yamate-cho, Suita, Osaka 564-8680, Japan

Hagen Schimmel

LightTrans GmbH, Jena D-07745, Germany

Frank Wyrowski

Friedrich Schiller University Jena, Jena D-07743, Germany

Received March 22, 2003; revised manuscript received May 8, 2003; accepted May 8, 2003

A novel method for simulating field propagation is presented. The method, based on the angular spectrum of plane waves and coordinate rotation in the Fourier domain, removes geometric limitations posed by conventional propagation calculation and enables us to calculate complex amplitudes of diffracted waves on a plane not parallel to the aperture. This method can be implemented by using the fast Fourier transformation twice and a spectrum interpolation. It features computation time that is comparable with that of standard calculation methods for diffraction or propagation between parallel planes. To demonstrate the method, numerical results as well as a general formulation are reported for a single-axis rotation. © 2003 Optical Society of America

OCIS codes: 050.1960, 350.5500, 090.1970, 000.3860.

1. INTRODUCTION

Developments in computer technology in the past few decades have created a revolution in the field of wave optics. Today our desktop computers can easily simulate optical diffraction by an aperture. The complex amplitudes in simulations are typically sampled on an equidistant grid. These simulations of diffraction are usually based on well-known scalar theories such as the Rayleigh–Sommerfeld formula, the Fresnel–Kirchhoff formula, and the Fresnel and Fraunhofer approximations of the latter. Another important method for computing optical diffraction is to use the angular spectrum of plane waves.[1] This method, accompanied by the fast-Fourier-transformation (FFT) algorithm, plays an important role in numerical simulations of optical diffraction and propagation. However, these methods share a common constraint in simulating diffraction: The screen or plane on which light waves diffracted by an aperture are calculated must be parallel to the aperture. No tilted screens or tilted apertures are allowed in standard formulations. To get rid of this limitation, diffraction by a tilted aperture has been investigated in some studies: Fraunhofer diffraction in Refs. 2–5 and Fresnel diffraction in Ref. 6. Furthermore, in the context of creating image holograms, Leseberg has suggested using rotational transformation of complex amplitudes in the Fourier domain in order to calculate object waves diffracted by tilted apertures.[7] However, we have found no complete formulations or results on such rotation in the literature.

New methods of simulation for optical diffraction and propagation with fewer constraints and higher performance are needed to improve optical techniques such as diffractive optics and digital holography, which allow us to measure[8] and create[9] complex amplitudes of light waves emitted by three-dimensional objects. In this paper we treat the formulation and numerical simulation of diffraction by an aperture onto an inclined plane, i.e., we calculate complex amplitudes at sampling points placed on a plane not parallel to the aperture. Although our major interest lies in three-dimensional displays,[10] the technique presented is useful in any wave-optical simulation concerning tilted planes.

2. BASIC THEORY AND FORMULATION

A. Basic Idea and Concept

Two coordinate systems are used in this investigation. One is the (x, y, z) source coordinate system, in which the complex amplitude $g(x, y)$ of a light wave is initially defined in the $(x, y, 0)$ plane. This plane is referred to as the source plane in this paper. The other system is the reference coordinate system $(\hat{x}, \hat{y}, \hat{z})$ at a distance d from the source coordinates, in which the complex amplitude $f(\hat{x}, \hat{y})$ of the propagated field is finally obtained in the $(\hat{x}, \hat{y}, 0)$ plane, which is referred to as the reference plane.

Figure 1 illustrates the specified coordinate systems with the source and reference planes and geometries cor-

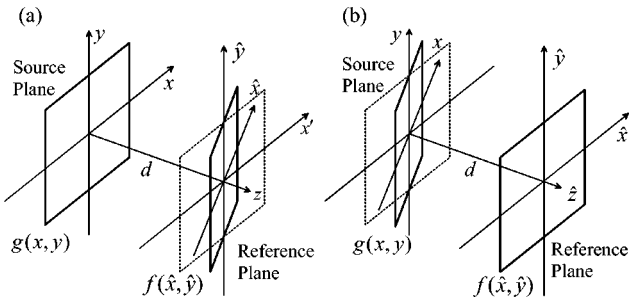

Fig. 1. Definition of coordinate system and schemes for (a) a tilted screen and (b) a tilted aperture.

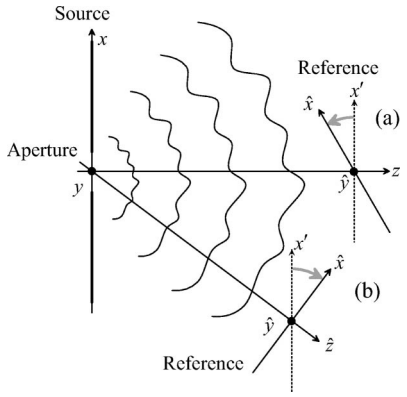

Fig. 2. Geometry for (a) a tilted screen and (b) a tilted aperture.

responding to (a) a tilted screen and (b) a tilted aperture. In (a), the source plane is perpendicular to the z axis, while the reference plane is not. The inverse situation is depicted in (b). Figure 2 shows schemes (a) and (b) from Fig. 1 depicted for a common aperture placed in the source plane. Figure 2(a) illustrates the situation for a tilted screen and Fig. 2(b) for a tilted aperture.

In both schemes the calculation of diffraction consists of two essential steps. For the inclined reference plane, light diffracted by the aperture is propagated to an intermediate plane $(x', \hat{y})$ that is parallel to the source plane. This calculation can be carried out with conventional methods based on the traditional diffraction theory. Next the calculated field given as complex amplitudes on $(x', \hat{y})$ is decomposed into plane waves by Fourier transformation. The expanded plane waves are reassembled in the tilted reference plane $(\hat{x}, \hat{y})$ and then combined again by using an inverse Fourier transformation. This step is referred to as coordinate rotation in the Fourier domain. The same procedure is generally applicable to a tilted source plane, as shown in Fig. 2(b); i.e., source complex amplitudes are propagated with conventional methods, followed by coordinate rotation.

In either scheme, the most essential and significant operation is the coordinate rotation in the Fourier domain, which will be described in the following subsection.

B. Coordinate Rotation in the Fourier Domain

In this subsection, assume that $d = 0$, i.e., the two coordinates share the origin, so that we can concentrate on the formulation of the coordinate rotation. If the two-dimensional complex amplitude $g(x, y, 0)$ is given in the source plane, the spectrum $G(u, v)$ is defined by

$$G(u, v) = \mathcal{F}\{g(x, y)\} = \int\int_{-\infty}^{\infty} g(x, y)\exp[-i2\pi(ux + vy)]\mathrm{d}x\mathrm{d}y \quad (1)$$

and the inverse transformation by

$$g(x, y) = \mathcal{F}^{-1}\{G(u, v)\} = \int\int_{-\infty}^{\infty} G(u, v)\exp[i2\pi(ux + vy)]\mathrm{d}u\mathrm{d}v. \quad (2)$$

Equation (2) can be interpreted as a superimposition of plane waves:

$$u(x, y, z = 0; u, v) = G(u, v)\exp[i2\pi(ux + vy)]. \quad (3)$$

$G(u, v)$ expresses the complex amplitude of the plane wave. The same plane wave with a complex amplitude A and a wave vector $\mathbf{k}$ can be defined in general as

$$u(x, y, z = 0; \mathbf{k}) = A\exp\left[i\frac{2\pi}{\lambda}(k_x x + k_y y)\right], \quad (4)$$

with

$$\mathbf{k} = \frac{2\pi}{\lambda}[k_x \quad k_y \quad k_z]. \quad (5)$$

Therefore $|\mathbf{k}| = 2\pi/\lambda$ and $k_x^2 + k_y^2 + k_z^2 = 1$. By comparing Eq. (3) with Eq. (4), wave vector $\mathbf{k}$ can be associated with Fourier frequencies (u, v) in the source plane by

$$\mathbf{k} = 2\pi[u \quad v \quad w(u, v)], \quad (6)$$

with $w(u, v) = (\lambda^{-2} - u^2 - v^2)^{1/2}$.

Let us now turn to the field in the reference plane, which is denoted $f(\hat{x}, \hat{y})$. Its spectrum is given by

$$F(\hat{u}, \hat{v}) = \mathcal{F}\{f(\hat{u}, \hat{v})\} = \int_{-\infty}^{\infty} f(\hat{x}, \hat{y})\exp[-i2\pi(\hat{u}\hat{x} + \hat{v}\hat{y})]\mathrm{d}\hat{x}\mathrm{d}\hat{y}. \quad (7)$$

Similarly to obtaining Eq. (4), we obtain

$$\hat{\mathbf{k}} = 2\pi[\hat{u} \quad \hat{v} \quad \hat{w}(\hat{u}, \hat{v})], \quad (8)$$

with $\hat{w}(\hat{u}, \hat{v}) = (\lambda^{-2} - \hat{u}^2 - \hat{v}^2)^{1/2}$.

The wave vectors given in Eqs. (6) and (8) are defined respectively, in the (x, y, z) and $(\hat{x}, \hat{y}, \hat{z})$ coordinate systems. Therefore if the two fields represent the same wave, the wave vector expressed in one coordinate system can be transformed into the other by using ordinary coordinate-transformation procedures.

Suppose that $\mathbf{T}$ is a matrix used to transform the source coordinates into the reference coordinates; then the wave vectors can be transformed into each other by

$$\hat{\mathbf{k}} = \mathbf{T}\mathbf{k}, \qquad \mathbf{k} = \mathbf{T}^{-1}\hat{\mathbf{k}}. \quad (9)$$

When the inverse transformation matrix is given as

$$\mathbf{T}^{-1} = \begin{bmatrix} a_1 & a_2 & a_3 \\ a_4 & a_5 & a_6 \\ a_7 & a_8 & a_9 \end{bmatrix}, \quad (10)$$

we can associate the Fourier frequencies in the source coordinates with those in the reference coordinates as follows:

$$u = \alpha(\hat{u}, \hat{v}) = a_1\hat{u} + a_2\hat{v} + a_3\hat{w}(\hat{u}, \hat{v}),$$
$$v = \beta(\hat{u}, \hat{v}) = a_4\hat{u} + a_5\hat{v} + a_6\hat{w}(\hat{u}, \hat{v}). \quad (11)$$

Thus the spectrum in the reference coordinates is given by the spectrum in the source coordinates according to

$$F(\hat{u}, \hat{v}) = G(\alpha(\hat{u}, \hat{v}), \beta(\hat{u}, \hat{v})). \quad (12)$$

It appears as if it is possible to calculate the complex amplitude in the reference plane by inverse transformation of the spectrum $F(\hat{u}, \hat{v})$. However, a simple inverse Fourier transformation of $F(\hat{u}, \hat{v})$ does not provide correct results, because the total energy of the field is not conserved after rotational transformation, owing to the nonlinearity of the transformation in Eq. (11).

The energy of a plane wave in Eq. (3) in source coordinates, which have Fourier frequencies (u, v) to $(u + du, v + dv)$, is proportional to $|G(u, v)\exp[i2\pi(ux + vy)]|^2 du\,dv$, and therefore the total energy of the field is given by

$$E_{\text{total}} \propto \int\int_{-\infty}^{\infty} |G(u, v)|^2 du\,dv. \quad (13)$$

In the transformed spectrum $F(\hat{u}, \hat{v}) = G(\alpha(\hat{u}, \hat{v}), \beta(\hat{u}, \hat{v}))$, the energy factor of a plane wave with Fourier frequencies $(\hat{u}, \hat{v})$ to $(\hat{u} + d\hat{u}, \hat{v} + d\hat{v})$ is written as

$$|G(\alpha(\hat{u}, \hat{v}), \beta(\hat{u}, \hat{v}))|^2 |J(\hat{u}, \hat{v})| d\hat{u}\,d\hat{v},$$

where the Jacobian $J(\hat{u}, \hat{v})$ is defined as

$$J(\hat{u}, \hat{v}) = \frac{\partial\alpha}{\partial\hat{u}}\frac{\partial\beta}{\partial\hat{v}} - \frac{\partial\alpha}{\partial\hat{v}}\frac{\partial\beta}{\partial\hat{u}}$$
$$= (a_2a_6 - a_3a_5)\frac{\hat{u}}{\hat{w}(\hat{u}, \hat{v})} + (a_3a_4 - a_1a_6)\frac{\hat{v}}{\hat{w}(\hat{u}, \hat{v})} + (a_1a_5 - a_2a_4), \quad (14)$$

which is needed to compensate for the nonlinearity of the rotational transformation. Thus the total energy is written as

$$E_{\text{total}} \propto \int\int_{-\infty}^{\infty} |G(\alpha(\hat{u}, \hat{v}), \beta(\hat{u}, \hat{v}))|^2 |J(\hat{u}, \hat{v})| d\hat{u}\,d\hat{v}. \quad (15)$$

To obtain complex amplitudes of the field in the reference coordinates that posses the same energy as that in the source coordinates, the plane waves $F(\hat{u}, \hat{v})\exp[i2\pi(\hat{u}\hat{x} + \hat{v}\hat{y})]$ must be integrated as follows:

$$f(\hat{x}, \hat{y}) = \int\int_{-\infty}^{\infty} F(\hat{u}, \hat{v})\exp[i2\pi(\hat{u}\hat{x} + \hat{v}\hat{y})] \times |J(\hat{u}, \hat{v})| d\hat{u}\,d\hat{v}. \quad (16)$$

This is rewritten with the inverse Fourier transformation and yields

$$f(\hat{x}, \hat{y}) = \mathcal{F}^{-1}\{F(\hat{u}, \hat{v})|J(\hat{u}, \hat{v})|\}. \quad (17)$$

When waves are paraxial in the reference coordinates [i.e., fields propagate in the $\hat{z}$ direction as shown in Fig. 1(b)], $\hat{u}$ and $\hat{v}$ are much smaller than $\hat{w}(\hat{u}, \hat{v})$. As a result, the first and second terms of the Jacobian in Eq. (14) can be ignored. In that case,

$$J(\hat{u}, \hat{v}) \simeq (a_1a_5 - a_2a_4) \quad (18)$$

is a good approximation.

On the other hand, when the waves are paraxial in the source coordinates, the Jacobian remaining after the approximation is a little complex, as described in Appendix A, but all terms that include the Fourier frequencies can be ignored. As a result, the integration of the rotated spectrum for the paraxial waves is reduced to the inverse Fourier transformation

$$f(\hat{x}, \hat{y}) \propto \mathcal{F}^{-1}\{F(\hat{u}, \hat{v})\}. \quad (19)$$

We refer to this as the paraxial approximation in the coordinate rotation.

3. SINGLE-AXIS ROTATION OF THE REFERENCE COORDINATES

In this section we treat the single-axis rotation of the reference coordinates, of which the scheme is depicted in Fig. 1(a), to verify the basic idea of rotating the coordinates in the Fourier domain.

A. Analytical Procedure

Suppose that a source field is given by $g(x, y)$ and its spectrum is given again by $G(u, v)$ in the source plane, but in this subsection the reference plane is assumed to be apart from the source plane; i.e., $d > 0$. In addition, suppose that $G_d(u, v)$ denotes the source spectrum in an intermediate plane, which is parallel to the source plane, and that its coordinates share the origin with the reference coordinates. One can choose an analytical or a numerical method from some conventional algorithms of field propagation to calculate fields in the intermediate plane, because this propagation is translational and is independent of the step in the coordinate rotation. In this paper we choose a standard formula of the angular spectrum of plane waves given as follows:

$$G_d(u, v) = G(u, v)\exp[i2\pi d(\lambda^{-2} - u^2 - v^2)^{1/2}]. \quad (20)$$

The transformation matrix used to rotate coordinates on the y axis with the angle of φ is given as

$$\mathbf{T}^{-1} = \begin{bmatrix} \cos\varphi & 0 & \sin\varphi \\ 0 & 1 & 0 \\ -\sin\varphi & 0 & \cos\varphi \end{bmatrix}. \quad (21)$$

By substituting elements of matrix (21) into Eqs. (11) and (14), we can write the angular spectrum in the reference coordinates and the Jacobian, respectively, as follows:

$$F(\hat{u}, \hat{v}) = G_d(\hat{u}\cos\varphi + \hat{w}(\hat{u}, \hat{v})\sin\varphi, \hat{v}), \quad (22)$$

$$J(\hat{u}, \hat{v}) = \cos\varphi - \frac{\hat{u}}{\hat{w}(\hat{u}, \hat{v})}\sin\varphi. \quad (23)$$

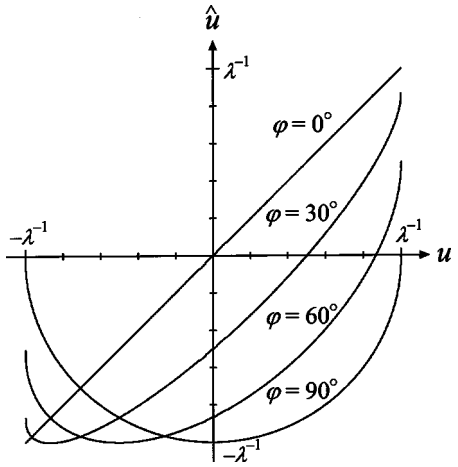

Fig. 3. Curves for transforming Fourier frequency u in source coordinates into $\hat{u}$ in reference coordinates; $v = 0$.

Therefore complex amplitudes in the reference plane are given by the inverse Fourier transformation

$$f(\hat{x}, \hat{y}) = \mathcal{F}^{-1}\left\{ G_d(\hat{u}\cos\varphi + \hat{w}(\hat{u}, \hat{v})\sin\varphi, \hat{v}) \times \left| \cos\varphi - \frac{\hat{u}}{\hat{w}(\hat{u}, \hat{v})}\sin\varphi \right| \right\}. \quad (24)$$

In the case of paraxial waves or small rotation angles, the second term on the right-hand side of Eq. (23) can be ignored. As a result, complex amplitudes in the paraxial approximation (19) are written as

$$f(\hat{x}, \hat{y}) \propto \mathcal{F}^{-1}\{G_d(\hat{u}\cos\varphi + \hat{w}(\hat{u}, \hat{v})\sin\varphi, \hat{v})\}. \quad (25)$$

B. Numerical Procedure

Equation (24) is rigorous in an analytic sense. However, the transformation in Eq. (22) causes numerical problems. One problem is the distortion of the equidistant sampling grid. For a fast calculation of diffraction for practical purposes, the FFT algorithm is commonly used to calculate $G(u, v)$ from $g(x, y)$ and $f(\hat{x}, \hat{y})$ from $F(\hat{u}, \hat{v})$. The FFT algorithm, however, works only for an equidistant sampling grid. Since the inverse function $\hat{u} = \alpha^{-1}(u, 0)$, as well as the function $u = \alpha(\hat{u}, 0)$ itself, is a nonlinear function as shown in Fig. 3, even if $G(u, v)$ and $G_d(u, v)$ are evenly sampled, the spacing of the sampling points for the transformed spectrum is not equal. As a result, some method of interpolation must be introduced into the sampled $F(\hat{u}, \hat{v})$ to calculate $f(\hat{x}, \hat{y})$ by FFT.

Furthermore, the transformation from Eq. (22) also causes a shift in the center frequency in the spectrum $F(\hat{u}, \hat{v})$. When $u = 0$ and $v = 0$ in the source coordinates, the corresponding reference frequency $\hat{u} = \alpha^{-1}(0, 0)$ does not equal zero. This can be interpreted to be a carrier frequency observed in the tilted reference coordinates. If one wants to calculate the diffracted waves in the reference plane by FFT, this nonzero carrier frequency should be eliminated, because the FFT algorithm does not work effectively for spectrums sampled far from zero frequency. Figure 4 shows the procedure used to eliminate the carrier frequency in the reference coordinates. Assume that the center frequency is $u_0 (=0)$ in the source spectrum, as shown in Fig. 4(a), and that $\hat{u}_0 (\neq 0)$ is the carrier frequency after rotation, as shown in Fig. 4(b). For an efficient conversion by FFT, another coordinate $u' = \hat{u} - \hat{u}_0$ should be introduced, as shown in Fig. 4(c). This results in complex amplitudes in the reference coordinates, which are given as

$$f(\hat{x}, \hat{y}) = \mathcal{F}^{-1}\{F(u', \hat{v})|J(u', \hat{v})|\}\exp[i2\pi\hat{u}_0 x]. \quad (26)$$

The carrier frequency $\hat{u}_0$ is possibly too high to be sampled in a given sampling scheme in the reference plane. Even in this case, the intensity distribution $|f(\hat{x}, \hat{y})|^2$ can be easily obtained, because the carrier frequency is included only as a phase factor of $\exp(i2\pi\hat{u}_0 x)$. Moreover, when one wants to consider the factor of the carrier frequency, it can be multiplied after inverse FFT.

C. Numerical Examples for Single-Axis Rotation

We prepared three numerical examples for the source amplitude $g(x, y)$ to verify the theory and evaluate numerical accuracy. We calculated complex amplitudes in a reference plane at $z = d$, which was rotated at an angle φ on the y axis, as shown in Fig. 5.

Parameters of the three samples are summarized in Table 1. Sample A is a paraxial Gaussian wave with a constant phase (i.e., the wave's waist) in the source plane. This is an example of a simple paraxial wave with smooth amplitude distribution. Sample B is a plane wave diffracted by a rectangular aperture in the source plane.

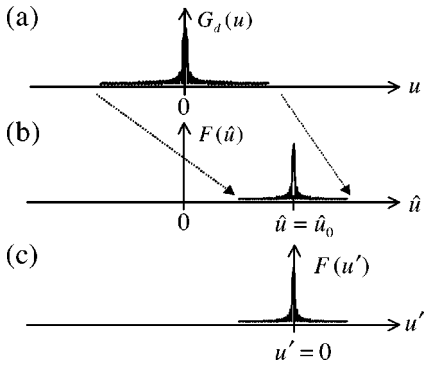

Fig. 4. Schematic diagram of spectrum shift: (a) spectrum in source coordinates, (b) reference coordinates, and (c) shift of spectral origin.

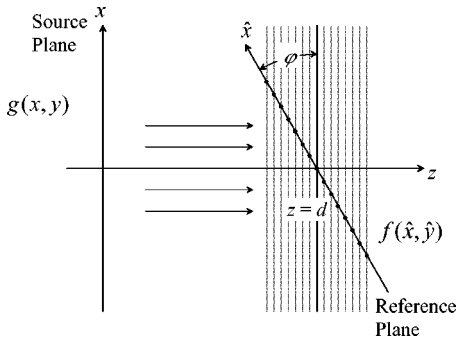

Fig. 5. Schematic setup for numerical simulation of single-axis rotation. One-dimensional rigorous amplitudes for comparison are calculated at sampling points (dots).

Table 1. Summary of Parameters Used for Numerical Simulations

$g(x, y)$	Sampling		
	Number	Pitch	d
Sample A, Gaussian	256	20 μm	10 mm
Sample B, rectangle aperture	256	20 μm	30 mm
Sample C, Gaussian with quadratic phase	512	5 μm	10 mm

The amplitude distribution of this wave is not smooth in the reference plane because of the fringe pattern. Sample C is also Gaussian, but it has a spherical phase in the source plane to simulate a Gaussian beam behind a lens with a focal length of 15 mm. This phase brings asymmetry as well as nonparaxiality into the distribution of the complex amplitudes in the tilted reference plane placed near the focal point.

D. Numerical Accuracy

As mentioned at the beginning of Subsection 3.B, approximations are not applied in the derivation of Eq. (24); i.e., the equation itself is rigorous. However, the interpolation of the sampled spectrum, which is necessary for the numerical calculation, causes numerical errors. Therefore the accuracy as well as the computation time of the numerical calculation is dependent on the method of interpolation. According to the sampling theorem, the sinc interpolation should provide the most accurate results, but the sinc interpolation is generally a very time-consuming method. Therefore we examine other interpolation methods in this section.

The numerical accuracy of the coordinate rotation was evaluated as signal-to-noise ratio (SNR) of rotated complex amplitudes defined as

$$\mathrm{SNR} = \frac{\int\int_{\infty} |f(\hat{x}, \hat{y})|^2 \mathrm{d}\hat{x}\mathrm{d}\hat{y}}{\int\int_{\infty} |f(\hat{x}, \hat{y}) - \alpha f_{\mathrm{rig}}(\hat{x}, \hat{y})|^2 \mathrm{d}\hat{x}\mathrm{d}\hat{y}}, \quad (27)$$

where $f_{\mathrm{rig}}(\hat{x}, \hat{y})$ is the distribution of complex amplitudes calculated by another rigorous method described below. In most cases, magnitude of the field is of no concern, and accuracy in the field form is of interest to us. Therefore a scale factor α maximizing SNR is defined as follows:

$$\alpha = \frac{\int\int_{\infty} f(\hat{x}, \hat{y}) f^*_{\mathrm{rig}}(\hat{x}, \hat{y}) \mathrm{d}\hat{x}\mathrm{d}\hat{y}}{\int\int_{\infty} |f_{\mathrm{rig}}(\hat{x}, \hat{y})|^2 \mathrm{d}\hat{x}\mathrm{d}\hat{y}}. \quad (28)$$

A rigorous calculation of complex amplitudes in the tilted reference plane is a serious problem because of its mathematical complexity. In almost all cases it seems to be impossible to obtain analytically rigorous solutions of the field in a tilted plane, and therefore we adopted a numerical approach. Figure 5 shows how we obtained the exact amplitudes in the tilted plane in this paper. Complex amplitudes were calculated on many planes perpendicular to the z axis and placed before and behind the position d; then the resultant amplitudes at sampling points were stitched along side the tilted reference plane. Although the resulting amplitudes may also create numerical errors, the accuracy of the method is high enough to provide a reference for comparison with complex amplitudes calculated by the proposed coordinate rotation. In addition, calculating exact amplitudes with this method was possible only for a one-dimensional distribution because of the long computation time.

Figure 6 shows SNRs measured numerically for a rotation angle of 30° in various interpolation algorithms of the Fourier spectrum. "nth" and "Cubic 8" indicate the nth-order iterated linear interpolation and the cubic-interpolation algorithms at 8 points,[11] respectively. The cubic interpolation almost always results in the best SNRs. These SNRs exceeded 50 dB for all samples with an angle of 30°.

In Fig. 7, SNRs measured in the cubic interpolation are shown in relation to the rotation angles. In samples A and B, the paraxial approximation of Eq. (25) gives the same SNRs as Eq. (24), whereas in sample C, the SNR calculated with the approximation decreases with an increase in rotation angle. The reason for this is clear: samples A and B are paraxial waves, whereas sample C, which has a definite beam waist, deviates from the paraxial condition. Thus the accuracy of numerical cal-

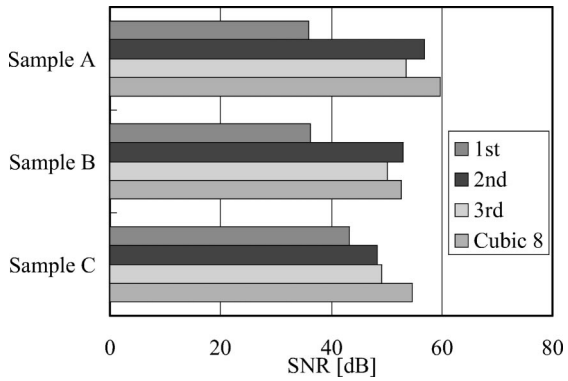

Fig. 6. SNRs in one-dimensional amplitudes for several interpolation algorithms. Here nth and Cubic 8 stand for nth iterative linear interpolation and cubic interpolation at 8 points, respectively. The rotation angle is 30°.

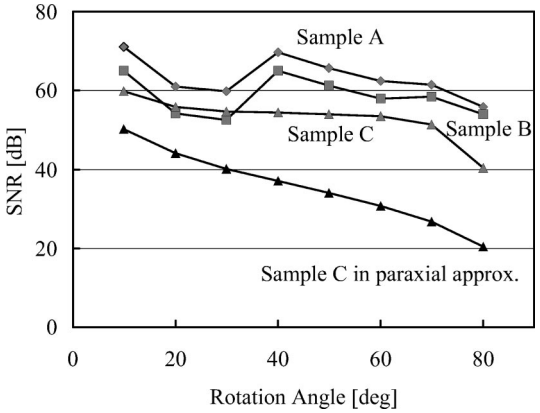

Fig. 7. SNR versus rotation angle. Cubic interpolation at 8 points is used in calculation.

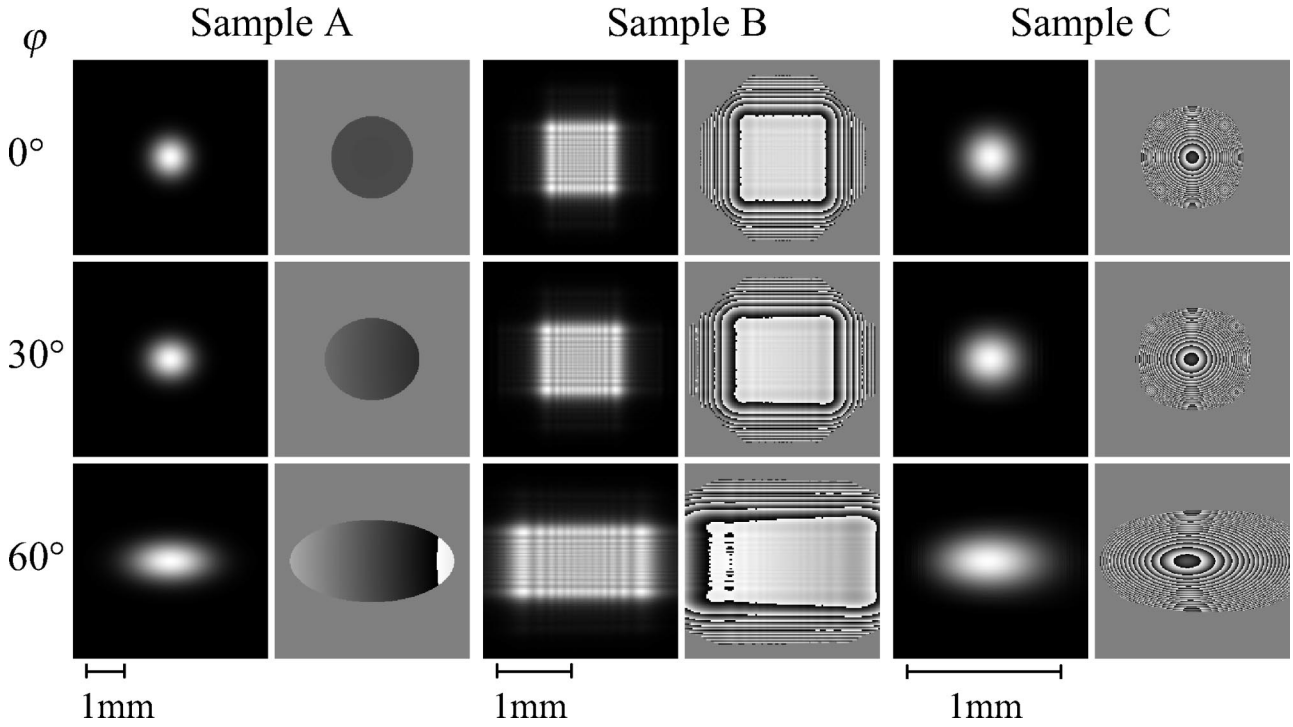

Fig. 8. Two-dimensional distribution of amplitudes and phase calculated on tilted reference planes. The phase factor due to the carrier frequency appearing on the tilted plane is eliminated in depicted phase images.

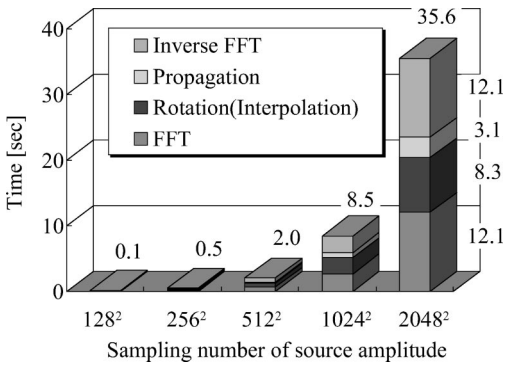

Fig. 9. Computation time for rotation and translational propagation. Measurements were made by using a Pentium III processor with 1 GHz frequency.

culation obtained by Eq. (25) drops with increasing degree of the rotation angle.

E. Two-Dimensional Results and Computation Time

Figure 8 shows the two-dimensional distributions of complex amplitudes for numerical samples A–C. The left and right columns for each sample depict amplitude and phase distribution, respectively. Note that the carrier frequency $\hat{u}_0$ mentioned in Subsection 3.B has been eliminated in the phase distributions.

The computation time for rotation accompanied by translational propagation was measured on an Intel Pentium III processor at 1 GHz. Figure 9 shows the time at different numbers of sampling points. In the measurement, the single-axis rotation was again calculated with cubic interpolation. The results of the computation time approximately agree with those of FFT, i.e., $n \log n$ for n samplings. This is attributed to the fact that two iterations of the FFT consume most of the processing time and the rest of the time is spent on interpolation and propagation, with computational costs that are proportional to n.

4. DISCUSSION

As shown in Fig. 3, the curves for transformation of frequency u into $\hat{u}$ open upward with positive values of φ and open downward with negative φ. Therefore the curves have a minimum value or a maximum value except for the case $\varphi = 0$. In some cases of large-angle rotation, this causes a "fold in the spectrum" in the reference coordinates. For example, when $\varphi = 90°$ in Fig. 3, two source frequencies $+u'$ and $-u'$ are assigned to an identical frequency $\hat{u}'$ of the reference spectrum. This means that the source spectrum is folded at its origin; i.e., both negative and positive frequency ranges in the source coordinates are projected onto the same range of the reference frequency.

The spectral fold originates in a group of plane waves that propagates from the region $\hat{z} > 0$ to the region $\hat{z} < 0$ in reference coordinates, as shown in the following. In the single-axis rotation, the frequency transformation is written as

$$\hat{u} = u \cos\varphi - w(u, v)\sin\varphi, \tag{29}$$

$$\hat{w} = u \sin\varphi + w(u, v)\cos\varphi. \tag{30}$$

The maximum and the minimum values are given at u satisfying $d\hat{u}/du = 0$, and thus

$$u \sin\varphi + w(u, v)\cos\varphi = 0, \tag{31}$$

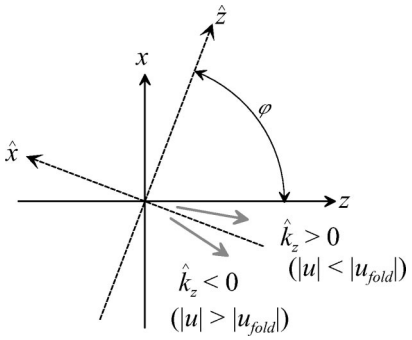

Fig. 10. Schematic depiction of the spectral fold. Each side with respect to the maximum or minimum value in frequency transformation curves corresponds to the sign of the $\hat{k}_z$ element of wave vectors in the reference coordinates.

and the z element of the wave vector in the reference coordinates is given by substituting Eq. (30) into Eq. (8) as follows:

$$\hat{k}_z(u, v) = 2\pi[u \sin\varphi + w(u, v)\cos\varphi]. \tag{32}$$

If $u = u_{\mathbf{fold}}$ satisfies the condition defined in Eq. (31), $u_{\mathbf{fold}}$ leads to $\hat{k}_z(u_{\mathbf{fold}}, v) = 0$. Therefore the sign of $\hat{k}_z$ changes at $u = u_{\mathbf{fold}}$ when u increases or decreases. The plane wave with a frequency $|u| < |u_{\mathbf{fold}}|$ in the source coordinates consequently propagates in the direction $\hat{z} > 0$, and vice versa. This relation is depicted in Fig. 10. Accordingly, the spectral fold means that two plane waves having an opposite sign of $\hat{k}_z$ to each other, i.e., having a mirrorlike symmetry with respect to the reference plane, contribute to the same plane.

This spectral fold does not occur in our numerical examples, because the spectrum is folded at $|u_{\mathrm{fold}}| = w(0, v)\cos\varphi$ in the single-axis rotation, and thus $|u_{\mathrm{fold}}| = \cos\varphi/\lambda$ in $v = 0$. In the examples presented, the broadest source spectrum is provided in $u = \pm 0.063/\lambda$ from Sample C, whereas $|u_{\mathrm{fold}}| = 0.174/\lambda$ even in the maximum rotation angle of 80°.

5. CONCLUSION

A method for calculating complex amplitudes of a diffracted wave on an inclined screen as well as on a wave diffracted by an inclined aperture was suggested. This method features a computation time that is comparable with that of standard methods in which a reference plane is parallel to a source plane. The procedure of this method can be summarized as follows: First calculate the spectrum of the source amplitude by FFT, then rotate the coordinate system in which the spectrum is given, and finally reintegrate the spectrum in rotated coordinates by using inverse FFT with a Jacobian because of the nonlinearity of the rotational transformation of the spectrum.

In the examples of single-axis rotation, SNRs of complex amplitudes on the tilted reference plane are measured by comparing them with rigorous results. In the one-dimensional distribution of complex amplitudes, these SNRs exceeded 50 dB in almost all examples and rotation angles. Two-dimensional distributions of complex amplitudes in the rotated reference plane were calculated for these examples, and the computation time was measured on a Pentium III processor at 1 GHz. The computation time was similar to that of FFT, for example, 35.6 s in the case of 2048^2 sampling points.

Finally, a physical interpretation for the spectral fold was discussed in relation to the propagation direction of plane waves in the reference coordinate system.

APPENDIX A: PARAXIAL APPROXIMATION IN THE SOURCE COORDINATES

When the inverse rotation matrix $\mathbf{T}^{-1}$ is defined by Eq. (10), assume that the rotation matrix is given by

$$\mathbf{T} = \frac{1}{|\mathbf{T}^{-1}|}\begin{bmatrix} A_1 & A_2 & A_3 \\ A_4 & A_5 & A_6 \\ A_7 & A_8 & A_9 \end{bmatrix}. \tag{A1}$$

Here A_i is a cofactor of the matrix $\mathbf{T}^{-1}$, and A_i's in the third column are associated with the matrix $\mathbf{T}^{-1}$ by

$$A_3 = (-1)^{(1+3)}\begin{vmatrix} a_2 & a_3 \\ a_5 & a_6 \end{vmatrix} = a_2a_6 - a_3a_5, \tag{A2}$$

$$A_6 = (-1)^{(3+2)}\begin{vmatrix} a_1 & a_3 \\ a_4 & a_6 \end{vmatrix} = a_3a_4 - a_1a_6. \tag{A3}$$

$$A_9 = (-1)^{(3+3)}\begin{vmatrix} a_1 & a_2 \\ a_4 & a_5 \end{vmatrix} = a_1a_5 - a_2a_4. \tag{A4}$$

Thus the Jacobian (14) is rewritten by using the cofactors:

$$J(\hat{u}, \hat{v}) = A_3\frac{\hat{u}}{\hat{w}} + A_6\frac{\hat{v}}{\hat{w}} + A_9. \tag{A5}$$

Moreover, the first term of the Jacobian is rewritten by transforming frequencies $(\hat{u}, \hat{v}, \hat{w})$ into (u, v, w) through the matrix $\mathbf{T}$:

$$A_3\frac{\hat{u}}{\hat{w}} = A_3\frac{A_1u + A_2v + A_3w}{A_7u + A_8v + A_9w}. \tag{A6}$$

If a field is paraxial in the source coordinate, i.e., if it propagates in almost the z direction, the frequency w is much larger than u and v. Therefore

$$A_3\frac{\hat{u}}{\hat{w}} = A_3\frac{A_1u/w + A_2v/w + A_3}{A_7u/w + A_8v/w + A_9} \simeq \frac{{A_3}^2}{A_9}, \tag{A7}$$

is a good approximation. With the same procedure, the second term of the Jacobian (A5) is approximated to

$$A_6\frac{\hat{v}}{\hat{w}} \simeq \frac{{A_6}^2}{A_9}. \tag{A8}$$

As a result, when fields are paraxial in the source coordinates, the paraxial approximation of coordinate rotation is given by

$$J(\hat{u}, \hat{v}) \simeq \frac{{A_3}^2 + {A_6}^2 + {A_9}^2}{A_9}. \tag{A9}$$

ACKNOWLEDGMENT

This work is partly supported by Kansai University High Technology Research Center.

REFERENCES

1. J. W. Goodman, *Introduction to Fourier Optics*, 2nd ed. (McGraw-Hill, New York, 1996), Chap. 3.10.
2. G. Harburn, J. K. Ranniko, and R. P. Williams, "An aspect of phase in Fraunhofer diffraction patterns," Optik (Stuttgart) **48**, 321–328 (1977).
3. S. Ganci, "Fourier diffraction through a tilted slit," Eur. J. Phys. **2**, 158–160 (1981).
4. K. Patorski, "Fraunhofer diffraction patterns of tilted planar objects," Opt. Acta **30**, 673–679 (1983).
5. H. J. Rabal, N. Bolognini, and E. E. Sicre, "Diffraction by a tilted aperture: coherent and partially coherent cases," Opt. Acta **32**, 1309–1311 (1985).
6. D. Leseberg and C. Frère, "Computer-generated holograms of 3-D objects composed of tilted planar segments," Appl. Opt. **27**, 3020–3024 (1988).
7. D. Leseberg, "Computer-generated three-dimensional image holograms," Appl. Opt. **31**, 223–229 (1992).
8. Y. Takaki and H. Ohzu, "Hybrid holographic microscopy: visualization of three-dimensional object information by use of viewing angles," Appl. Opt. **39**, 5302–5308 (2000).
9. K. Matsushima and M. Takai, "Recurrence formulas for fast creation of synthetic three-dimensional holograms," Appl. Opt. **39**, 6587–6594 (2000).
10. K. Matsushima, H. Schimmel, and F. Wyrowski, "New creation algorithm for digitally synthesized holograms in surface model by diffraction from tilted planes," in *Practical Holography XVI and Holographic Materials VIII*, S. A. Benton, S. H. Stevenson, and T. J. Trout, eds., Proc. SPIE **4659**, 53–60 (2002).
11. T. M. Lehmann, C. Gönner, and K. Spitzer, "Large-sized local interpolators," in *Proceedings of The International Association of Science and Technology for Development (IASTED) Conference on Computer Graphics and Imaging* (ACTA Press, Calgary, Alberta, Canada, 1999), pp. 156–161.